nanomaterials

MDPI

*Supporting Information*

# High-Stability $Ti_3C_2$-QDs/$ZnIn_2S_4$/Ti(IV) Flower-Like Heterojunction for Boosted Photocatalytic Hydrogen Evolution

**Liqin Yang [1], Zhihong Chen [2,3], Xin Wang [1,2] and Mingliang Jin [1,2,*]**

[1] National Center for International Research on Green Optoelectronics, South China Academy of Advanced Optoelectronics, South China Normal University, Guangzhou 510006, China; yangliqin2019@126.com (L.Y.); wangxin@scnu.edu.cn (X.W.)
[2] International Academy of Optoelectronics at Zhaoqing, South China Normal University, Zhaoqing 526000, China; chenzhihong1227@sina.com
[3] Key Laboratory for Water Quality and Conservation of the Pearl River Delta, Ministry of Education, Institute of Environmental Research at Greater Bay, Guangzhou University, Guangzhou 510006, China
* Correspondence: jinml@scnu.edu.cn

## 1. Experimental

### *1.1. Characterization*

The morphology and structure of samples were observed by field-emission scanning electron microscopy (FESEM, ZEISS Gemini 500, Carl Zeiss, Germany) and transmission electron microscopy (TEM, JEM-2100HR, Tokyo, Japan). X-ray powder diffraction (XRD) and Fourier-transform infrared (FT-IR) patterns of the as-prepared samples were conducted on a Bruker D8 Advance X-ray diffractometer (Karlsruhe, Germany) with Cu K$\alpha$ X-ray source and a Thermo spectrometer, respectively, to expound the crystalline and chemical structure. The inductively coupled optical emission spectrometry (ICP-MS, Agilent 7800, Upland, CA, USA) was performed to analyze the composition of the samples. The chemical and valence states of involved elements were carried out by X-ray photoelectron spectroscopy (XPS, Thermo Fisher Scientific ESCALAB $Xi^+$, Waltham, MA, USA) with a monochromatic Al K-alpha radiation source. UV-vis diffuse reflectance spectroscopy (DRS) was measured from a UV-vis spectrophotometer (HITACHI U-41000, Tokyo, Japan) to obtain the optical property of the as-prepared samples.

The steady-state photoluminescence (PL) spectra were carried out on a fluorescence spectrometer (Hitachi F-4600, Tianjin, China). Time-resolved photoluminescence (TR-PL) spectra were recorded with a single photon counting spectrometer from Horiba Instrument, Fluorolog-3, Irvine, CA, USA. The time resolution was determined to be ps level from the instrument response function (IRF), and the TR-PL decay effective lifetimes ($\tau_{eff}$) of the sample is at ns level, so the influence of the instrument on the experimental results is negligible. In the TR-PL decay spectra measurement, the measured TR-PL decay curve is the convolution of the IRF and the ideal time decay curve, and the IRF has been deducted by the built-in software of the instrument. The specific surface area (BET) was examined by the $N_2$ adsorption-desorption experiments (Quantachrome Instruments, Shanghai, China). The electron paramagnetic resonance (EPR) spectra of liquid samples were recorded on a Brukera 300 spectrometer, Brooke, Germany.

### *1.2. Photoelectrochemical Measurements*

The photoelectrochemical tests of the as-prepared samples were performed on an electrochemical workstation (Shanghai, CHI660E, China) to explore the charge separation. In the process of testing, the prepared photocatalyst, Pt sheet and Ag/AgCl electrode (3 M KCl) were used as working, counter and reference electrodes, respectively. Typically, 5.0 mg photocatalyst and 10 μL Nafion (5 wt%) solution were added into the mixture of 400 μL water and isopropanol (3:1 v/v). After ultrasonic treatment for 60 min, a uniform colloidal solution was obtained. Finally, the colloidal solution was deposited on a clean FTO

with an area of 1 $cm^2$, and the working electrode was obtained after drying in the natural state. The 0.2 M of $Na_2SO_4$ aqueous solution and a Xe lamp (300 W) equipping a cut-off filter (AM 1.5) were used as the electrolyte and the light source in the measurements, respectively.

*1.3. Photocatalytic $H_2$ Production*

Briefly, 20 mg photocatalysts and 100 mL aqueous solution (0.35 M $Na_2S$/0.25 M $Na_2SO_3$) was added to a top-irradiation quartz photoreactor vessel with closed gas circulation and evacuation system and sealed with a rubber septum. Before the photocatalytic reaction, the photoreactor was vacuumed to eliminate air for 60 min and the circulating cooling water was connected to maintain the inside temperature. Then, it was irradiated by a 300-W Xe lamp equipped with a cut-off filter (AM 1.5) to provide the simulated sunlight irradiations (Perfect Light, Beijing, China). The produced $H_2$ was quantified by Labsolar-6A online photocatalytic analysis system (Perfect Light technology Co.LTD, Beijing, China) and gas chromatography (Techcomp GC7900, Shanghai, China, equipped with a thermal conductivity detector (TCD) and 5 Å molecular sieve columns). The calibration curve method was used for the quantitative analysis of $H_2$ production. The procedure of standardizing the calibration curve is as follows: under the identical atmosphere system as photocatalytic $H_2$ production, a series of different $H_2$ volume ratios were automatically injected and detected by GC to obtain a series of points for calibration ($H_2$ volume is used as abscissa and $H_2$ peak area in GC pattern is used as ordinate). Each calibration curve point is required to fall on the calibration curve as much as possible, and the correlation coefficient $r^2$ of the curve is greater than 0.999, ensuring the accuracy and linearity of the calibration curve. The raw data of points ($H_2$ volume vs $H_2$ peak area in GC pattern) was listed as follows:

| **$H_2$ volume (mL)** | **0.5** | **1** | **2** | **3** | **4** |
|---|---|---|---|---|---|
| $H_2$ peak area in GC pattern (uV*S) | 47,621 | 112,309 | 230,679 | 351,619 | 464,235 |

Finally, the $H_2$ evolution quantitative calibration curve in this work has been deduced as follows: $y = 118988 * x - 8582.4, r^2 = 0.9996$ (y refers to the $H_2$ peak area in GC pattern (uV*S), x refers to $H_2$ volume (mL), $r^2$ refers to correlation coefficient). The gas volume of each injection is 1 mL, and the activities of photocatalysts are compared using the average $H_2$ evolution rate in the first 4 h.

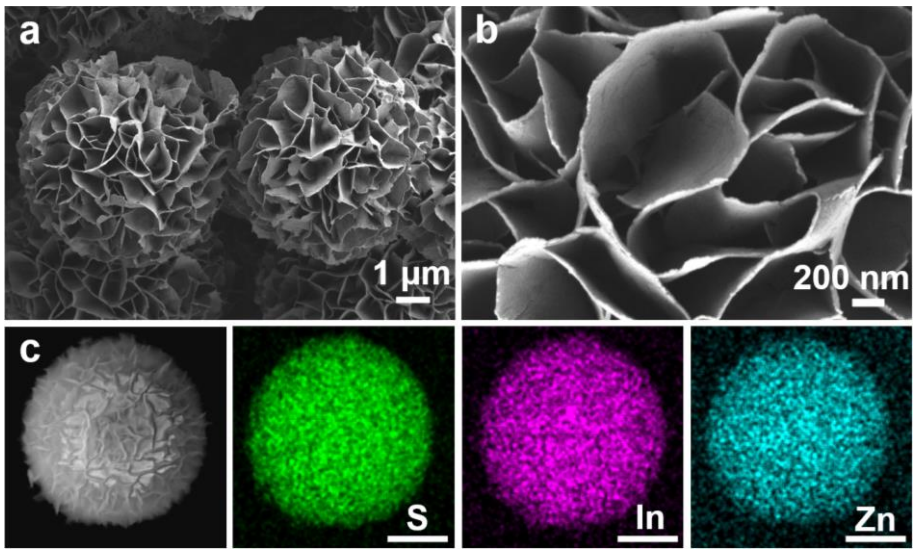


**Figure S1.** SEM images (**a**,**b**) and corresponding element (S, In and Zn) mappings (**c**) of ZIS.

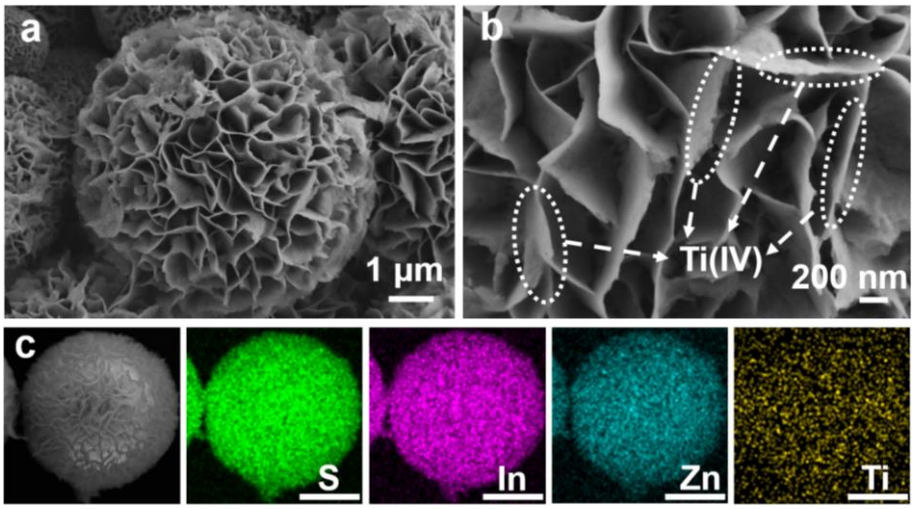


**Figure S2.** SEM images (**a**,**b**) and corresponding element (S, In, Zn and Ti) mappings (**c**) of ZIS/Ti(IV).

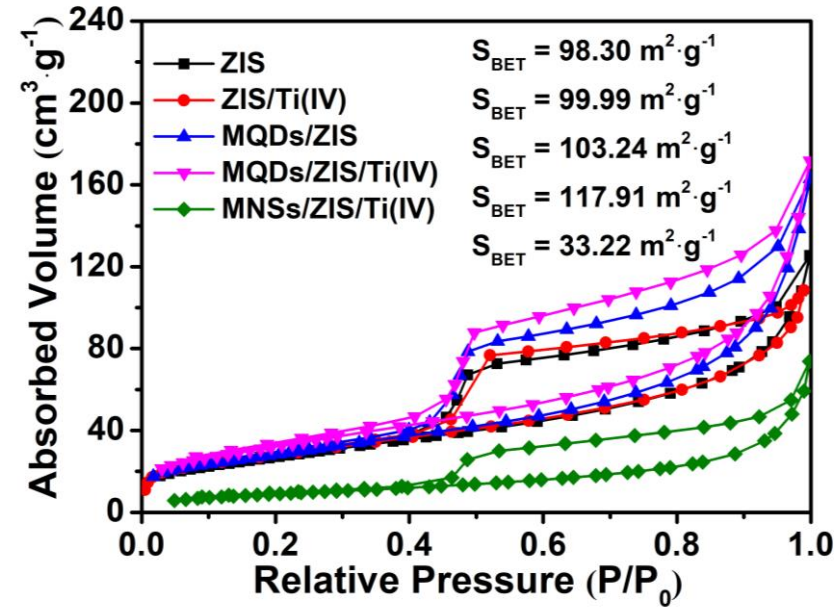


**Figure S3.** $N_2$ adsorption−desorption isotherms curves of ZIS, ZIS/Ti(IV), MQDs/ZIS, MQDs/ZIS/Ti(IV) and MNSs/ZIS/Ti(IV).

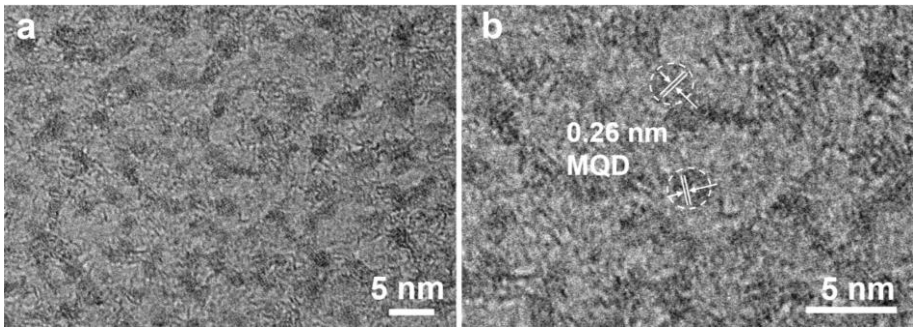


**Figure S4.** TEM images of MQDs (a) and enlarged portion (b) of MQDs TEM images.

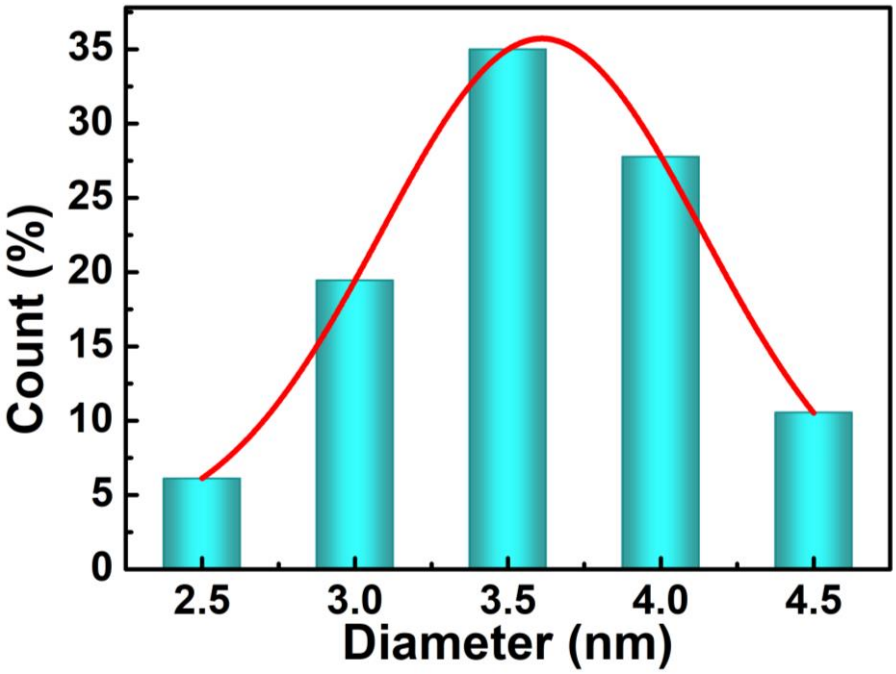


**Figure S5.** The diameter distribution of MQDs.

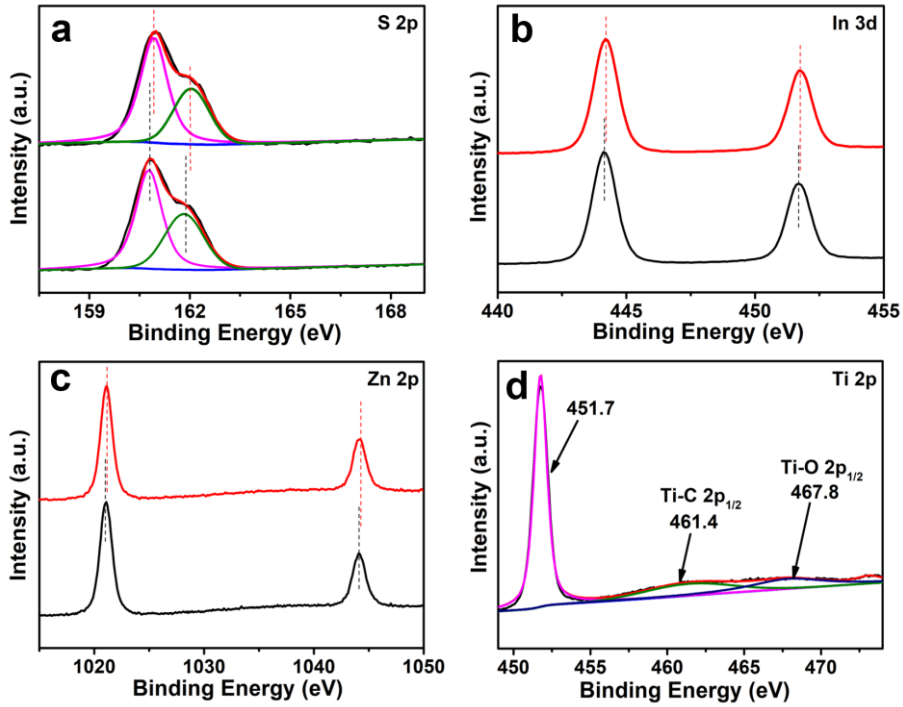


**Figure S6.** S 2p (**a**), In 3d (**b**), Zn 2p (**c**) and Ti 2p (**d**) XPS spectra of ZIS and ZIS/Ti(IV).

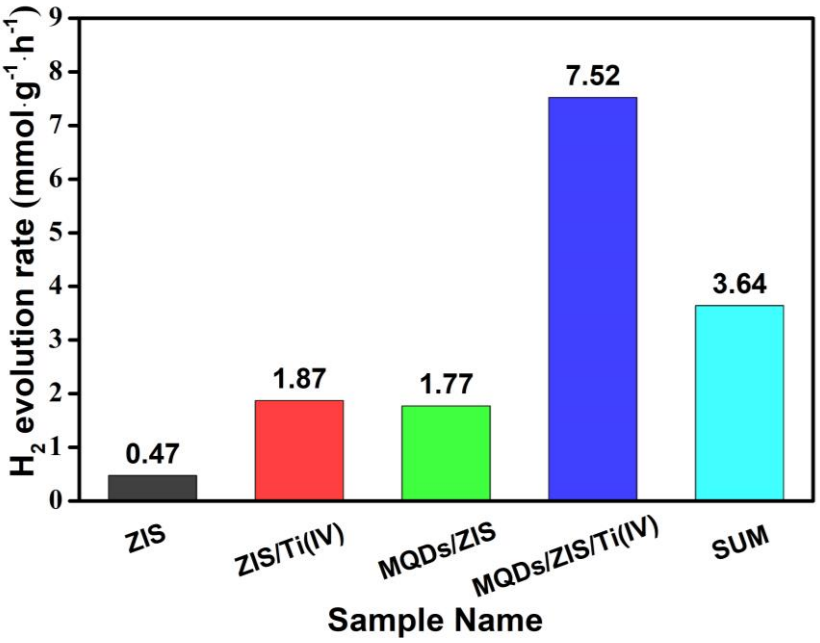


**Figure S7.** Histogram of average $H_2$ production rates of ZIS, ZIS/Ti(IV), MQDs/ZIS, MQDs/ZIS/Ti(IV) and the sum of ZIS/Ti(IV) and MQDs/ZIS.

a

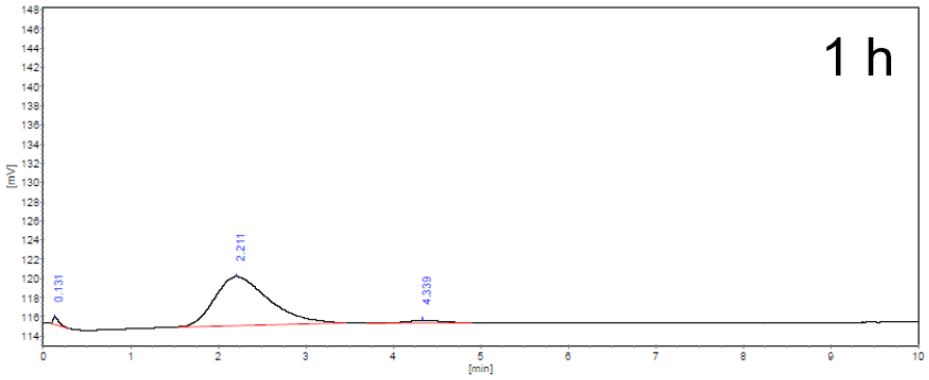


Analysis Results

| No. | Compound Name | R.Time [min] | Height [uV] | Area [uV*s] | Area% | Conc. [mg/mL] | Type |
|---|---|---|---|---|---|---|---|
| 1 | | 0.131 | 754 | 3780 | 1.6259 | 0.0000 | BB |
| 2 | H2 | 2.211 | 5071 | 219766 | 94.5199 | 0.0000 | BB |
| 3 | | 4.339 | 273 | 8961 | 3.8542 | 0.0000 | BB |
| | **Total:** | | **6098** | **232507** | **100.0000** | **0.0000** | |

b

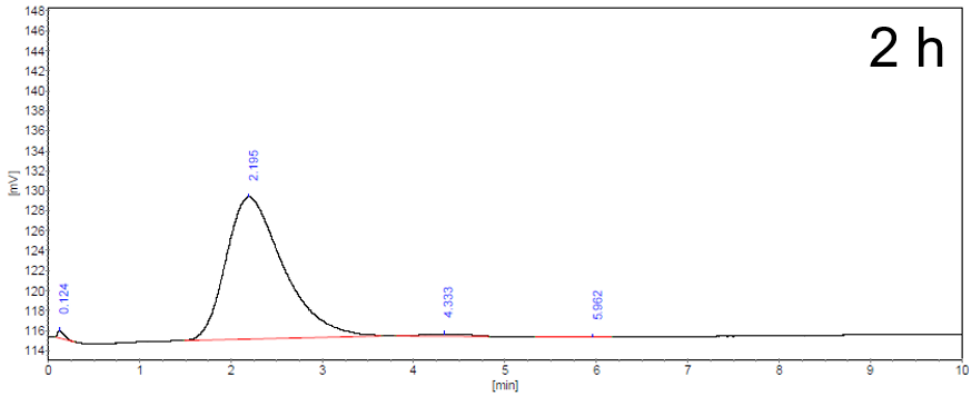


Analysis Results

| No. | Compound Name | R.Time [min] | Height [uV] | Area [uV*s] | Area% | Conc. [mg/mL] | Type |
|---|---|---|---|---|---|---|---|
| 1 | | 0.124 | 751 | 3697 | 0.5874 | 0.0000 | BB |
| 2 | H2 | 2.195 | 14158 | 616600 | 97.9556 | 0.0000 | BB |
| 3 | | 4.333 | 241 | 7680 | 1.2201 | 0.0000 | BB |
| 4 | | 5.962 | 32 | 1179 | 0.1873 | 0.0000 | BB |
| 5 | | 10.680 | 29 | 313 | 0.0497 | 0.0000 | BB |
| | **Total:** | | **15211** | **629469** | **100.0000** | **0.0000** | |

C

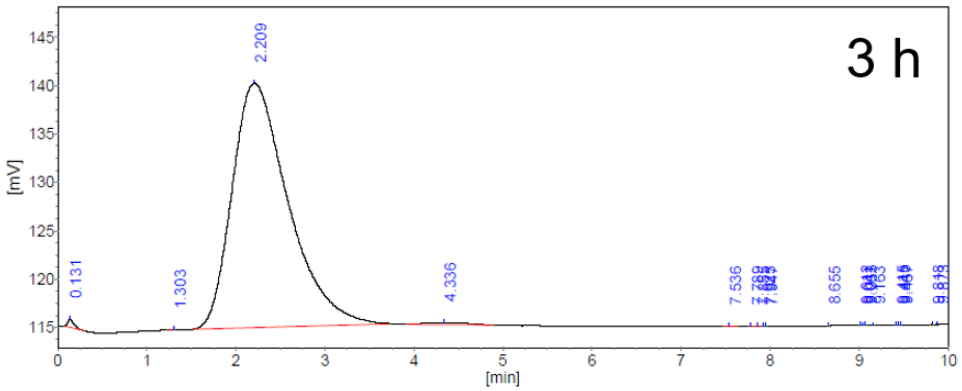


Analysis Results

| No. | Compound Name | R.Time [min] | Height [uV] | Area [uV*s] | Area% | Conc. [mg/mL] | Type |
|---|---|---|---|---|---|---|---|
| 1 | | 0.131 | 783 | 3908 | 0.3502 | 0.0000 | BB |
| 2 | | 1.303 | 29 | 91 | 0.0082 | 0.0000 | BB |
| 3 | H2 | 2.209 | 25239 | 1104034 | 98.9229 | 0.0000 | BB |
| 4 | | 4.336 | 252 | 7384 | 0.6616 | 0.0000 | BB |
| 5 | | 7.536 | 27 | 46 | 0.0041 | 0.0000 | BB |
| 6 | | 7.789 | 32 | 59 | 0.0052 | 0.0000 | BV |
| 7 | | 7.855 | 32 | 177 | 0.0159 | 0.0000 | VV |
| 8 | | 7.925 | 32 | 39 | 0.0035 | 0.0000 | VV |
| 9 | | 7.947 | 32 | 16 | 0.0015 | 0.0000 | VB |
| 10 | | 8.655 | 14 | 7 | 0.0006 | 0.0000 | BB |
| 11 | | 9.012 | 32 | 37 | 0.0033 | 0.0000 | BV |
| 12 | | 9.041 | 22 | 14 | 0.0012 | 0.0000 | VV |
| 13 | | 9.063 | 32 | 19 | 0.0017 | 0.0000 | VB |
| 14 | | 9.163 | 19 | 10 | 0.0009 | 0.0000 | BB |
| 15 | | 9.415 | 22 | 11 | 0.0010 | 0.0000 | BB |
| 16 | | 9.445 | 19 | 10 | 0.0009 | 0.0000 | BV |
| 17 | | 9.467 | 24 | 12 | 0.0011 | 0.0000 | VB |
| 18 | | 9.818 | 32 | 26 | 0.0023 | 0.0000 | BB |
| 19 | | 9.873 | 24 | 12 | 0.0011 | 0.0000 | BB |
| 20 | | 10.585 | 27 | 14 | 0.0012 | 0.0000 | BB |
| 21 | | 10.618 | 32 | 24 | 0.0021 | 0.0000 | BV |
| 22 | | 10.640 | 32 | 35 | 0.0031 | 0.0000 | VV |
| 23 | | 10.673 | 32 | 71 | 0.0064 | 0.0000 | VB |
| | **Total:** | | **26821** | **1116055** | **100.0000** | **0.0000** | |

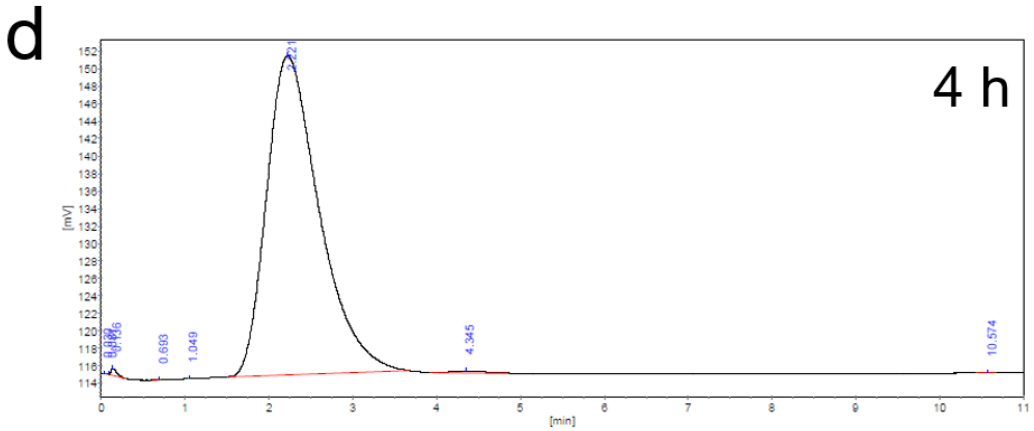


Analysis Results

| No. | Compound Name | R.Time [min] | Height [uV] | Area [uV*s] | Area% | Conc. [mg/mL] | Type |
|---|---|---|---|---|---|---|---|
| 1 | | 0.030 | 19 | 10 | 0.0006 | 0.0000 | BB |
| 2 | | 0.081 | 73 | 67 | 0.0042 | 0.0000 | BV |
| 3 | | 0.136 | 800 | 4003 | 0.2494 | 0.0000 | VB |
| 4 | | 0.693 | 27 | 104 | 0.0065 | 0.0000 | BB |
| 5 | | 1.049 | 15 | 6 | 0.0004 | 0.0000 | BB |
| 6 | H2 | 2.221 | 36463 | 1594854 | 99.3533 | 0.0000 | BB |
| 7 | | 4.345 | 218 | 5989 | 0.3731 | 0.0000 | BB |
| 8 | | 10.574 | 32 | 203 | 0.0126 | 0.0000 | BB |
| | **Total:** | | **37647** | **1605236** | **100.0000** | **0.0000** | |

**Figure S8. a–d.** The GC diagram of the best sample (MQDs/ZIS/Ti(IV)) at each time (1, 2, 3 and 4 h).

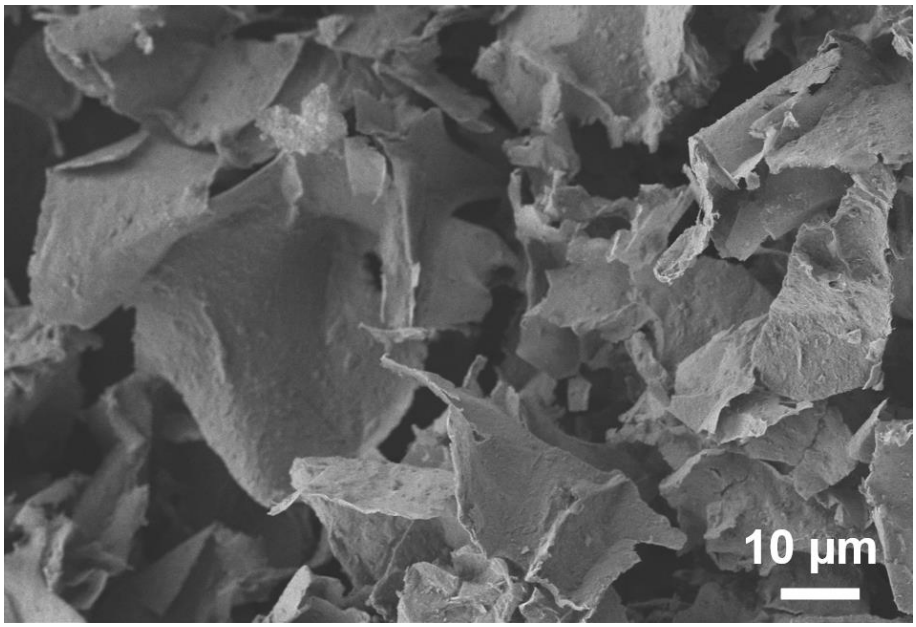


**Figure S9.** SEM image of MNSs.

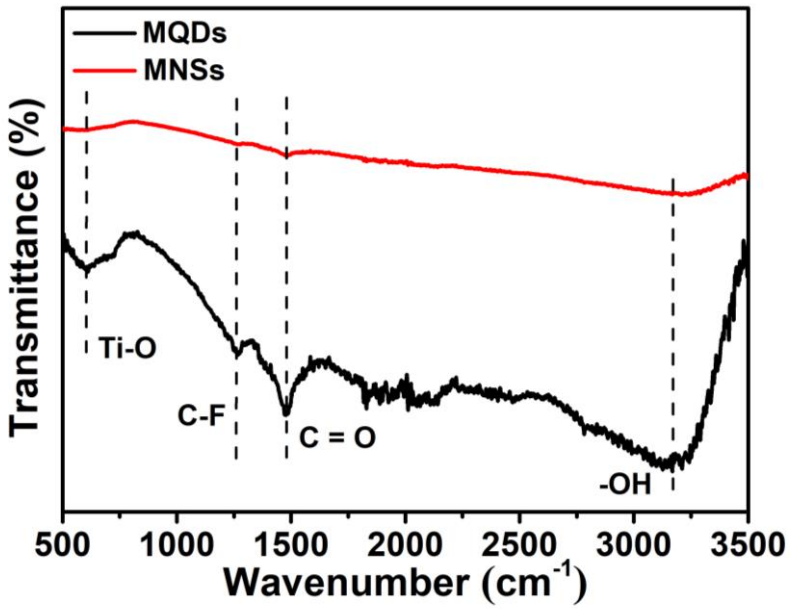


**Figure S10.** The FT-IR spectra of MQDs and MNSs.

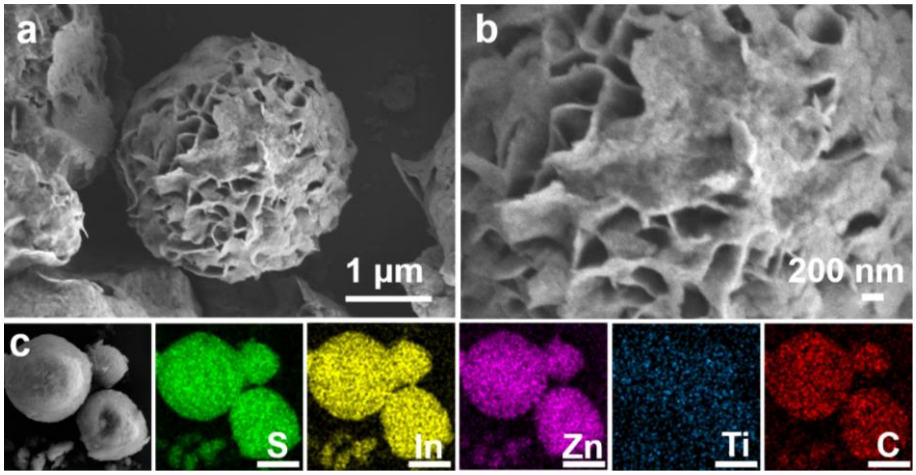


**Figure S11.** SEM images (**a**,**b**) and corresponding element (S, In, Zn, Ti and C) mappings (**c**) of MNSs/ZIS/Ti(IV).

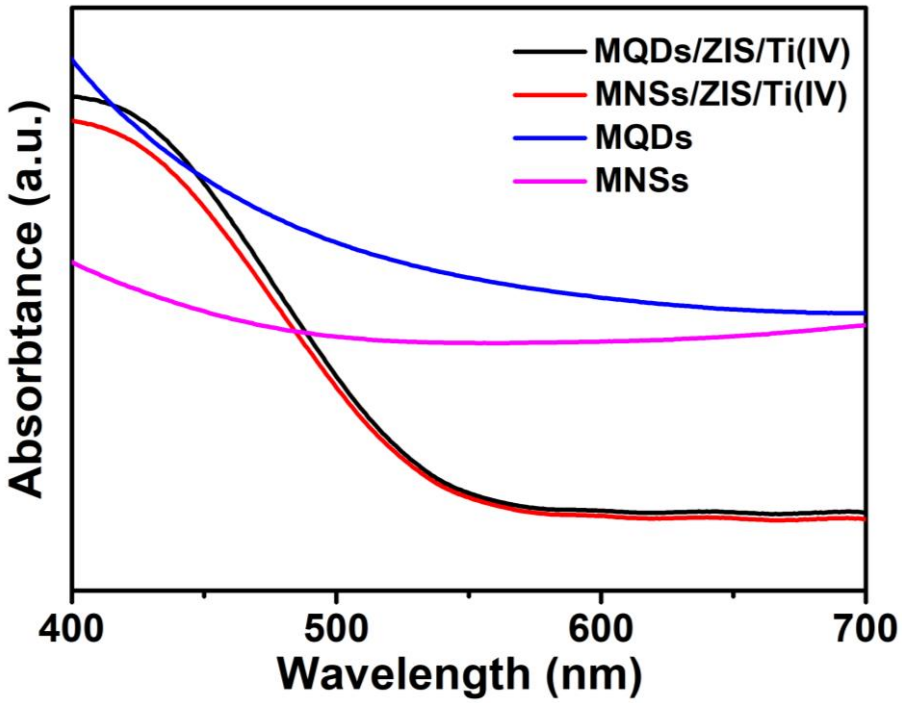


**Figure S12.** UV–vis diffuse reflectance spectra of MQDs/ZIS/Ti(IV), MNSs/ZIS/Ti(IV), MQDs and MNSs samples.

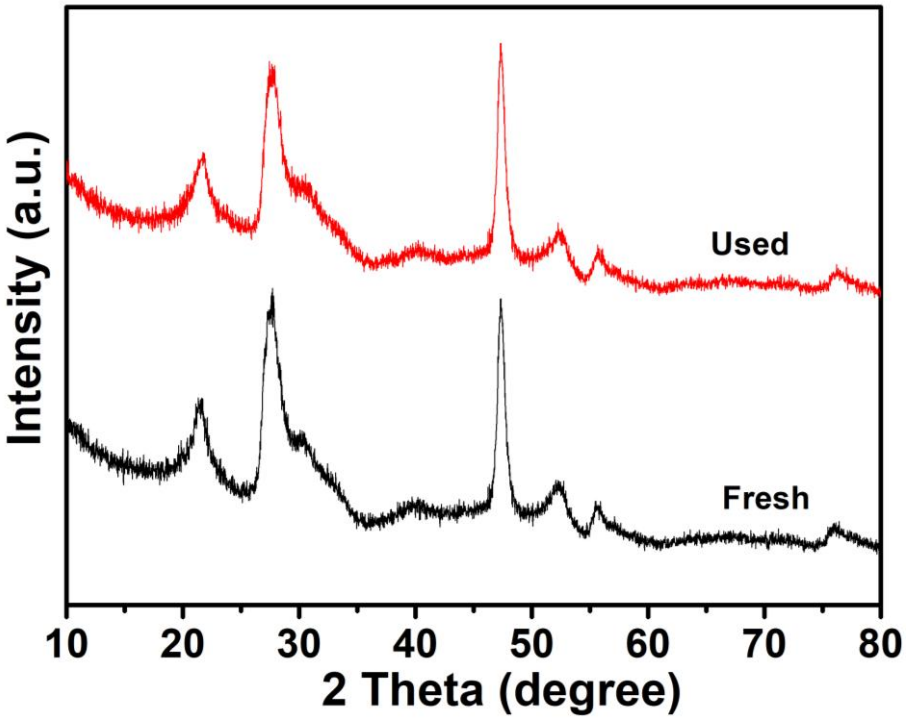


**Figure S13.** The XRD patterns of MQDs/ZIS/Ti(IV) fresh and after photocatalytic $H_2$ evolution test.

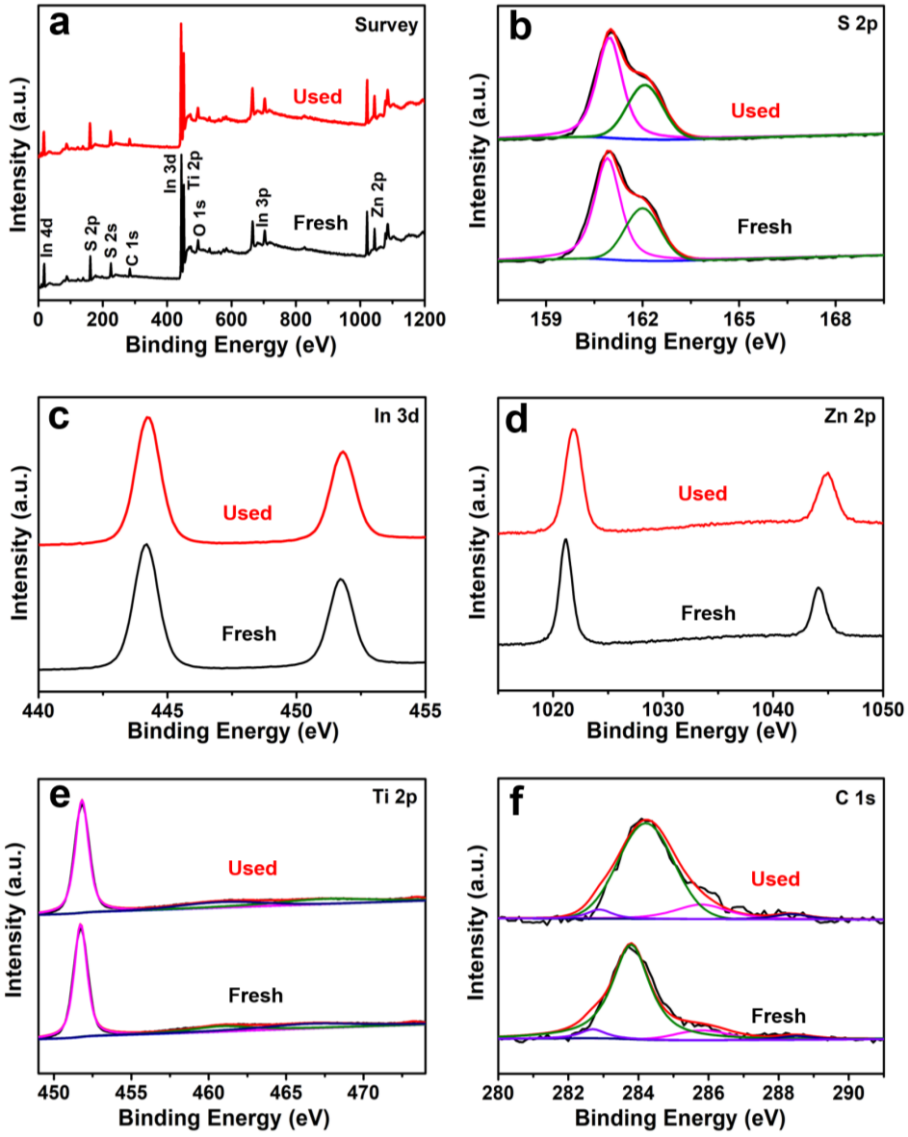


**Figure S14.** The XPS spectra of MQDs/ZIS/Ti(IV) fresh and after photocatalytic $H_2$ evolution test: survey (**a**), S 2p (**b**), In 3d (**c**), Zn 2p (**d**), Ti 2p (**e**) and C 1s (**f**).

**Table S1.** The photocatalytic $H_2$ evolution of ZIS, ZIS/Ti(IV), $MQDs_{(x)}$/ZIS, and $MQDs_{(x)}$/ZIS/Ti(IV) samples under simulated sunlight irradiation (AM 1.5).

| Samples | $H_2$ Peak Area in GC Pattern (uV*S) | | | | Quantitative Analysis of Photocatalytic $H_2$ Production Calibration Curve | Photocatalytic Activity ($mmol \cdot g^{-1} \cdot h^{-1}$) |
|---|---|---|---|---|---|---|
| | 1 h | 2 h | 3 h | 4 h | | |
| ZIS | 19,446 | 43,741 | 64,974 | 92,490 | $y = 118988 * x - 8582.4 r^2 = 0.9996$ y refers to the $H_2$ peak area in GC pattern (uV*S) x refers to $H_2$ volume (mL) $r^2$ refers to correlation coefficient | 0.47 |
| ZIS/Ti(IV) | 81,851 | 174,693 | 270,543 | 390,684 | | 1.87 |
| $MQDs_{(1)}$/ZIS | 49,065 | 106,299 | 162,497 | 227,366 | | 1.11 |
| $MQDs_{(2)}$/ZIS | 88,811 | 166,357 | 273,930 | 368,341 | | 1.77 |
| $MQDs_{(3)}$/ZIS | 69,054 | 165,730 | 246,141 | 368,315 | | 1.77 |
| $MQDs_{(4)}$/ZIS | 21,045 | 82,542 | 205,524 | 344,216 | | 1.65 |
| $MQDs_{(1)}$/ZIS/Ti(IV) | 163,254 | 380,614 | 646,975 | 923,286 | | 4.37 |
| $MQDs_{(2)}$/ZIS/Ti(IV) | 219,766 | 616,600 | 1,104,034 | 1,594,854 | | **7.52** |
| $MQDs_{(3)}$/ZIS/Ti(IV) | 97,544 | 297,011 | 485,846 | 691,635 | | 3.28 |
| $MQDs_{(4)}$/ZIS/Ti(IV) | 108,934 | 260,842 | 471,674 | 646,490 | | 3.07 |

**NOTE:** The 2 wt% MQDs doped ZIS and ZIS/Ti(IV) displays the highest photocatalytic $H_2$-production activity in MQDs(x)/ZIS and MQDs(x)/ZIS/Ti(IV) samples, respectively. Therefore, the sample with the best photocatalytic activity is selected as the representative to investigate their optical and physicochemical properties. In the text part, MQDs/ZIS and MQDs/ZIS/Ti(IV) are corresponded to $MQDs_{(2)}$/ZIS and $MQDs_{(2)}$/ZIS/Ti(IV), respectively.

**Table S2.** The ICP-MS test results of ZIS/Ti(IV) and MQDs/ZIS/Ti(IV) samples.

| Element | In ($mg \cdot g^{-1}$) | Zn ($mg \cdot g^{-1}$) | Ti ($mg \cdot g^{-1}$) |
|---|---|---|---|
| ZIS/Ti(IV) | 458.9 | 120.9 | 0.3 |
| MQDs/ZIS/Ti(IV) | 415.2 | 117.2 | 3.0 |

**Table S3.** The photocatalytic $H_2$ evolution compared with other works on ZIS photocatalysts integrated with quantum dots.

| Photocatalysts | Co-catalyst Metal | Photocatalytic Activity ($mmol \cdot g^{-1} \cdot h^{-1}$) | References |
|---|---|---|---|
| $Ti_3C_2$ MXene QDs/$ZnIn_2S_4$/Ti(IV) | free | **7.52** | This work |
| $CuInS_2$ QDs/$ZnIn_2S_4$ | 0.75 wt% of Pt | 1.04 | [S1] |
| CdTe QDs/$ZnIn_2S_4$ | free | 0.34 | [S2] |
| CdS/$MoS_2$ QDs/$ZnIn_2S_4$ | free | 2.11 | [S3] |
| $AgO_2$ QDs/$ZnIn_2S_4$ | 3 wt% of Pt | 0.47 | [S4] |
| BPQDs@$Cu_7S_4$/$ZnIn_2S_4$ | free | 0.89 | [S5] |
| MoC QDs/C/$ZnIn_2S_4$ | free | 1.13 | [S6] |

**Table S4.** The photocatalytic $H_2$ evolution of MQDs/ZIS/Ti(IV) and $MNSs_{(x)}$/ZIS/Ti(IV) samples under simulated sunlight irradiation (AM. 1.5).

| Samples | $H_2$ Peak Area in GC Pattern (uV*S) | | | | Quantitative Analysis of Photocatalytic $H_2$ Production Calibration Curve | Photocatalytic Activity ($mmol \cdot g^{-1} \cdot h^{-1}$) |
|---|---|---|---|---|---|---|
| | 1 h | 2 h | 3 h | 4 h | | |
| MQDs/ZIS/Ti(IV) | 219,766 | 616,600 | 1,104,034 | 1,594,854 | $y = 118988 * x - 8582.4$ | **7.52** |
| $MNSs_{(1)}$/ZIS/Ti(IV) | 122,533 | 243,689 | 364,789 | 492,713 | $r^2 = 0.9996$ y refers to the $H_2$ peak | 2.35 |
| $MNSs_{(2)}$/ZIS/Ti(IV) | 168,956 | 328,449 | 563,897 | 809,243 | area in GC pattern (uV*S)x refers to | 3.84 |
| $MNSs_{(3)}$/ZIS/Ti(IV) | 125,506 | 213,609 | 302,961 | 392,951 | $H_2$ volume (mL) | 1.88 |
| $MNSs_{(4)}$/ZIS/Ti(IV) | 103,470 | 190,106 | 265,768 | 343,816 | $r^2$ refers to correlation coefficient | 1.65 |

**Table S5.** The photocatalyst $H_2$ evolution of 4 cycling stability tests of MQDs/ZIS/Ti(IV) under simulated sunlight irradiation (AM 1.5).

| Cycle Index | $H_2$ Peak Area in GC Pattern (uV*S) | | | | Quantitative Analysis of Photocatalytic $H_2$ Production Calibration Curve | Photocatalytic Activity ($mmol \cdot g^{-1} \cdot h^{-1}$) |
|---|---|---|---|---|---|---|
| | 1 h | 2 h | 3 h | 4 h | | |
| 1st | 219,766 | 616,600 | 1,104,034 | 1,594,854 | $y = 118988 * x - 8582.4$ | 7.52 |
| 2nd | 382,210 | 776,262 | 1,151,478 | 1,556,524 | $r^2 = 0.9996$y refers to the $H_2$ peak area in | 7.34 |
| 3th | 433,124 | 839,545 | 1,180,133 | 1,547,258 | GC pattern (uV*S)x refers to $H_2$ volume | 7.30 |
| 4th | 418,276 | 808,624 | 1,175,932 | 1,499,172 | (mL)$r^2$ refers to correlation coefficient | 7.07 |

**Table S6.** The exponential decay-fitted parameters of the fluorescence lifetime of ZIS, ZIS/Ti(IV), MQDs/ZIS, MQDs/ZIS/Ti(IV) and MNSs/ZIS/Ti(IV).

| Samples | $A_1$ | $\tau_1$ | $A_2$ | $\tau_2$ | $\tau_{eff}$ |
|---|---|---|---|---|---|
| ZIS | 0.50312 | 0.4327 | 0.28178 | 11.56616 | 4.43 |

| | | | | | |
|---|---|---|---|---|---|
| ZIS/Ti(IV) | 0.85249 | 7.42244 | 0.85248 | 7.42151 | 7.42 |
| MQDs/ZIS | 0.49565 | 2.60739 | 0.09761 | 29.86587 | 7.09 |
| MQDs/ZIS/Ti(IV) | 0.17794 | 52.17659 | 0.25204 | 5.56178 | 24.85 |
| MNSs/ZIS/Ti(IV) | 0.1828 | 47.30022 | 1.07879 | 3.43148 | 9.79 |

## References


1. Cavdar, O.; Malankowska, A.; Amgar, D.; Mazierski, P.; Łuczak, J.; Lisowski, W.; Zaleska-Medynska, A. Remarkable visible-light induced hydrogen generation with ZnIn2S4 microspheres/CuInS2 quantum dots photocatalytic system. *International Journal of Hydrogen Energy* **2021**, *46*, 486–498.
2. Janani, R.; Sumathi, S.; Gupta, B.; Shaheer, A.R.M.; Ganapathy, S.; Neppolian, B.; Roy, S.C.; Channakrishnappa, R.; Paul, B.; Singh, S. Development of CdTe quantum dot supported ZnIn2S4 hierarchical microflowers for improved photocatalytic activity. *J. Environ. Chem. Eng.* **2022**, *10*, 107030.
3. Chen, W.; Yan, R.-Q.; Zhu, J.-Q.; Huang, G.-B.; Chen, Z. Highly efficient visible-light-driven photocatalytic hydrogen evolution by all-solid-state Z-scheme CdS/QDs/ZnIn2S4 architectures with MoS2 quantum dots as solid-state electron mediator. *Appl. Surf. Sci.* **2020**, *504*, 144406.
4. Xiao, Y.; Peng, Z.; Zhang, W.; Jiang, Y.; Ni, L. Self-assembly of Ag2O quantum dots on the surface of ZnIn2S4 nanosheets to fabricate p-n heterojunctions with wonderful bifunctional photocatalytic performance. *Appl. Surf. Sci*. **2019**, *494*, 519–531.
5. Zhang, Q.; Zhang, J.; Zhang, L.; Yang, F.; Li, L.; Dai, W.-L. Black phosphorus quantum dots facilitate carrier separation for enhancing hydrogen production over hierarchical Cu7S4/ZnIn2S4 composites. *Catal. Sci. Technol.* **2020**, *10*, 1030–1039.
6. Gao, F.; Zhao, Y.; Zhang, L.; Wang, B.; Wang, Y.; Huang, X.; Wang, K.; Feng, W.; Liu, A.P. Well Dispersed MoC Quantum Dots in Ultrathin Carbon Film as Efficient Co-catalyst for Photocatalytic H2 Evolution. *J. Mater. Chem. A* **2018**, *6*, 18979–18986.